A R C H I V E S O F M E T A L L U R G Y A N D M A T E R I A L S
Volume 53 2008 Issue 4

N. MOELANS*

A PHASE-FIELD MODEL FOR MULTI-COMPONENT AND MULTI-PHASE SYSTEMS

ZASTOSOWANIE MODELU PÓL FAZOWYCH DLA UKŁADÓW WIELOFAZOWYCH, WIELOSKŁADNIKOWYCH

An alternative phase-field model is presented for the simulation of microstructure evolution in polycrystalline materials existing of multiple phases and components. The model is able to treat concurrently phase transformations, diffusion controlled coarsening (Ostwald ripening) and grain growth. The equilibrium phase fractions and compositions are introduced using appropriate thermodynamic Gibbs energy expressions. Furthermore, the model allows to specify the energy and mobility, and their anisotropy, for each interface individually and the diffusion properties of the different phases. Simulation results are discussed for the coarsening of a simplified Cu/Cu-Sn solder joint with Cu_6Sn_5-precipitates.

Keywords: microstructure, soldering, thermodynamic modeling, simulation, coarsening, metals

Przedstawiono alternatywny model pól fazowych zastosowany do symulacji zmian mikrostruktury w materiałach polikrystalicznych w układach wielofazowych i wieloskładnikowych. Zaproponowany model uwzględnia jednocześnie przemiany fazowe oraz kontrolowany dyfuzyjnie rozrost ziaren (tzw. dojrzewanie Ostwalda). Przedstawiono i przedyskutowano wyniki uproszczonej symulacji przeprowadzonej dla połączenia lutownego Cu/Cu-Sn z wydzieleniem Cu_6Sn_5.

1. Introduction

Many materials of industrial relevance are multi-component, consist of several phases with a different crystal structure and/or several grains with a different crystal orientation. Especially at elevated temperatures, where grain boundary movement and diffusion are considerable, the structures coarsen in time. Examples are grain growth and Ostwald ripening (both driven by interfacial energy), and the growth of intermetallic precipitates in a supersaturated matrix or an intermetallic layer between 2 substrates (driven by bulk energy). As a result, the material properties change in time, which may or may not be desired.

The phase-field approach has proven to be powerful for simulating the morphological changes for different processes, such as solidification, precipitation, martensitic transformations and coarsening [1-3]. Characteristic for phase-field models is that interfaces are assumed to be diffuse and have a finite width. One advantage is that phase-field models can tackle the evolution of arbitrarily complex morphologies. While early applications were mostly qualitative and for simplified materials, currently, much more attention is given to quantitative aspects. To reduce the computational requirements, so called 'thin interface' phase-field models have been developed. In these models the interfacial width is considered as a numerical parameter that can be modified for numerical reasons without affecting other system properties, such as interfacial energy, diffusion behavior or bulk thermodynamic properties. In this way, it has become feasible to perform accurate 3D simulations for realistic dimensions.

A 'thin-interface' formulation for grain growth in single-phase systems was recently introduced by the author [4]. This model can treat arbitrary misorientation and inclination dependence and allows us a high controllability of the accuracy of the simulation results. In the present paper, this model for grain growth in single-phase materials is combined with a 'thin-interface' approach for multi-component alloys, which was originally developed by Tiaden et al. [5] and Kim et al. [6]. The reader is referred to [4] and [5-8] for a theoretical derivation of the approach.

* K.U.LEUVEN, DEPT. OF METALLURGY AND MATERIALS ENGINEERING, LEUVEN, BELGIUM

2. Model formulation

Model variables

Assume a polycrystalline material with C components and different phases α,β, ...ρ with different crystal orientations. It is furthermore assumed that pressure, temperature and molar volume are constant. The different grains are represented by a large set of non-conserved order parameter fields, which are a function of time t and spatial coordinates $\mathbf{r}$,

$$\vec{\eta} = (\eta_{\alpha 1}(\mathbf{r},t), \eta_{\alpha 2}, ..., \eta_{\beta 1}, \eta_{\beta 2}, ..., \eta_{\rho i}, ...).$$

The first symbol in the subscript refers to the different phases (with a different crystal structure) and the second to different crystal orientations of the same phase. Furthermore, C-1 independent conserved composition fields, representing the local mol fraction of one of the components, are used

$$\vec{x} = (x_1(\mathbf{r},t), ..., x_k, ..., x_{C-1}).$$

Thermodynamic Description

The total Gibbs energy F of a heterogeneous system is formulated as a functional of all field variables

$$\begin{aligned} &F(\eta_{\alpha 1}, ..., \eta_{\beta i}, ..., \eta_{\rho i}, ..., x_1, x_2, ..., x_{C-1}) \\ &\quad = F_{int} + F_{bulk} \\ &= \int_V \left[m f_0(\eta_{\alpha 1}, ..., \eta_{\beta i}, ..., \eta_{\rho i}, ...) + \frac{\kappa(\vec{\eta})}{2} \sum_{\rho i} (\nabla \eta_{\rho i})^2 \right] dV \\ &\quad + \int_V f_b(\eta_{\alpha 1}, ..., \eta_{\beta i}, ..., \eta_{\rho i}, ..., x_1, x_2, ..., x_{C-1}) dv \end{aligned} \tag{1}$$

where $\sum_{\rho i} *$ indicates a sum over all order parameter fields. The energy functional consists of a bulk contribution F_{bulk} and an interfacial contribution F_{int}. The functional f_0 in the interfacial contribution is a fourth order polynomial of the order parameter fields

$$f_0(\vec{\eta}) = \sum_{\rho i} \left(\frac{\eta_{\rho i}^4}{4} - \frac{\eta_{\rho i}^2}{2} \right) + \frac{\gamma(\vec{\eta})}{2} \sum_{\rho i} \sum_{\sigma} \sum_{j \neq \rho i} \eta_{\rho i}^2 \eta_{\sigma j}^2 + \frac{1}{4}, \tag{2}$$

with degenerate minima, where $f_0 = 0$, at

$$\begin{aligned} &(\eta_{\alpha i}, ..., \eta_{\alpha i}, ..., \eta_{\beta i}, ...) = (1, ..., 0, ..., 0...), ..., \\ &(0, ..., 1, ..., 0, ...), ..., (0, ..., 0, ...1, ...), ... \end{aligned} \tag{3}$$

corresponding to the different phases and different crystal orientations. The model parameters κ, γ and m are related to the interfacial free energy γ_{int} (a physical property of the system) and the diffuse interface width ℓ_{int} (chosen based on numerical considerations) as

$$\gamma_{\text{int}} = g(\gamma) \sqrt{m\kappa} \tag{4}$$

and

$$\ell_{\text{int}} = \sqrt{\frac{\kappa}{m f_{0,\text{int}}(\gamma)}} \tag{5}$$

where $g(\gamma)$ and $f_{0,\text{int}}(\gamma)$ are evaluated numerically as described in [4]. To distinguish between different interfacial energies for different phase boundaries, κ and γ can be formulated as a function of the order parameter fields [4].

Following [5-8], the bulk free energy density f_b in the phase-field free energy description (1) is related to the molar Gibbs energies $G_m^\rho\ (x_1, \ldots, x_{C-1}, T*)$ of the different phases as a function of composition and for temperature $T*$ as

$$f_b = \sum_\rho \left(\phi_\rho \frac{G_m^\rho(\vec{x}^\rho, T^*)}{V_m} \right) + \sum_{k=1}^{C-1} \tilde{\mu}_k \left(x_k - \sum_\rho \phi_\rho x_k^\rho \right), \tag{6}$$

with V_m the molar volume, ϕ_ρ the local fraction of phase ρ, $\tilde{\mu}_k$ the inter-diffusion potential for component k and $\vec{x}^\rho = (x_1^\rho, ..., x_{C-1}^\rho)$ *virtual* composition fields for the different phases. Different from the models in [5-8], the sum of the local values of the order parameter fields may be different from 1 at interfaces. Therefore, the local phase fractions ϕ_ρ are calculated from the order parameter fields as

$$\phi_\rho = \frac{\sum_i \eta_{\rho i}^a}{\sum_i \eta_{\rho i}^a + \sum_{\sigma \neq \rho} \sum_i \eta_{\sigma i}^a}, \tag{7}$$

with a an even natural number (usually $a = 2$ or 4 satisfies, for systems far from equilibrium it may be necessary to take a larger than 4).

The virtual composition fields x_k^ρ are calculated from the real composition fields x_k, so that

$$x_k = \sum_\rho \phi_\rho x_k^\rho, \quad k = 1...C-1 \tag{8}$$

and

$$\tilde{\mu}_k = \frac{1}{V_m} \frac{\partial G_m^\alpha}{\partial x_k^{alpha}} = ... = \frac{1}{V_m} \frac{\partial G_m^\rho}{\partial x_k^\rho} = ..., \quad k = 1...C-1, \tag{9}$$

although the inter-diffusion potentials $\tilde{\mu}_k$ may vary from point to point in space. It can be verified for relations (6)-(9) that within the bulk of a phase ρ, $x_k = x_k^\rho$ and $G_m(x_k) = G_m^\rho(x_k^\rho)$. Only at interfaces, the virtual composition fields differ from the real composition field. Thanks to restriction (9), f_b does not contribute to the interfacial energy. As a consequence, interfacial energy and thickness can be chosen independently by changing the parameters κ, γ and m, and without affecting the bulk properties.

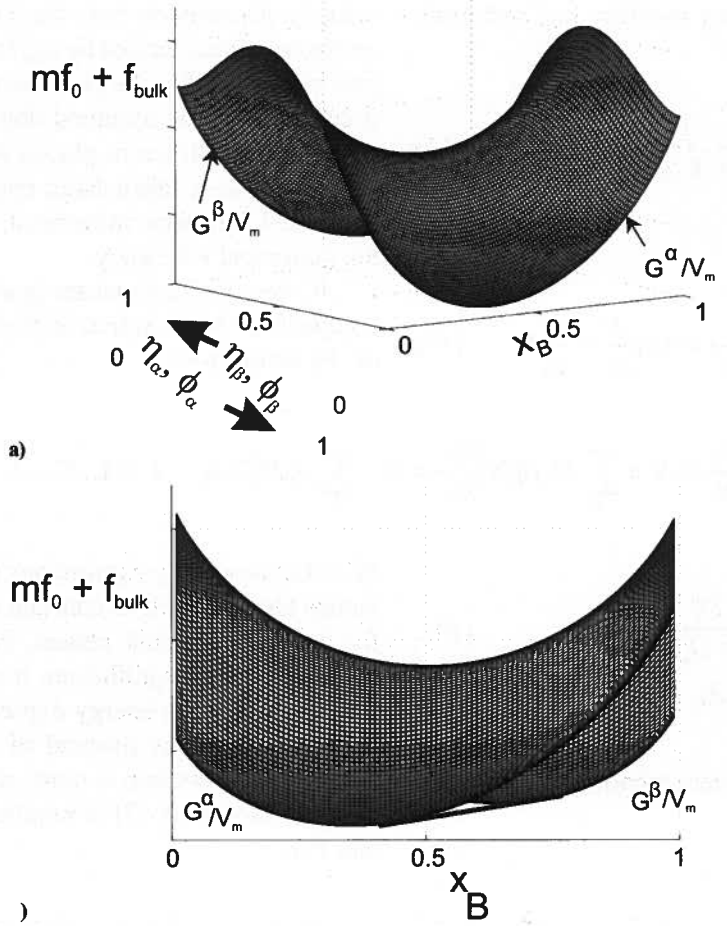

Fig. 1. (a) 3-dimensional representation of the homogeneous part in the phase field free energy for a system with 2 phases and 2 components, represented by the field variables $\eta_{\alpha 1}, \eta_{\beta 1}$ and $x_B \cdot \phi_\alpha$ and ϕ_β are the phase fractions of respectively the α and β phase. (b) Projection of the free energy landscape from figure (a) on the plane $x_B - f_{hom}$. The common tangent which connects the compositons of the coexisting phases for the two-pase region is indicated

Figure 1a shows a possible shape of the homogeneous terms $f_{hom} = mf_0(\eta_{\alpha 1}, \eta_{\beta 1}) + f_{bulk}(\eta_{\alpha 1}, \eta_{\beta 1}, x_B)$ in the phase field free energy (1), assuming a system with two phases and two components (represented by 2 phase fields $\eta\alpha 1$ and $\eta_{\beta 1}$ and 1 composition variable x_B). For $(\eta_{\alpha 1} = \alpha 1, \eta_{\beta 1} = 0)$, the homogeneous free energy reduces to $G^\alpha(x_B)/V_m$ and for $(\eta_{\alpha 1} = 0, \eta_{\beta 1} = 1)$ to $G^\beta(x_B)/V_m$. For other values of the order parameter fields, the homogeneous free energy interpolates between the two composition dependent Gibbs free energy curves using a function of the order parameter fields with relative minima at $(\eta_{\alpha 1} = 1, \eta_{\beta 1} = 0)$ and $(\eta_{\alpha 1} = 0, \eta_{\beta 1} = 1)$ and a maximum in between. In this way the order parameters will vary between 0 and 1 only at interfaces. In Figure 1b, the 3D energy landscape is projected on the $x_B - f_{hom}(\eta_{\alpha 1}, \eta_{\beta 1}, x_B)$ – plane. The equilibrium composition and fraction of coexisting phases, which can be obtained from the Gibbs free energy curves using the classical common tangent construction and lever rule, are reproduced in phase field simulations, except when precipitates or grains are so small that interfacial energy becomes important.

Evolution equations

The evolution of the non-conserved order parameter fields is assumed to follow

$$\frac{\partial \eta_{\rho i}}{\partial t} = -L(\vec{\eta})\frac{\delta F(\vec{\eta}, \vec{x})}{\delta \eta_{\rho i}} = -L(\vec{\eta})\left(m\frac{\partial f_0(\vec{\eta})}{\partial \eta_{\rho i}} - \kappa(\vec{\eta})\nabla^2\eta_{\rho i} + \frac{\partial f_b(\vec{\eta}, \vec{x})}{\partial \eta_{\rho i}}\right), \forall \eta_{\rho i}, \tag{10}$$

where L is a parameter related to the interface kinetics. For grain boundaries between grains of a same phase, L is related to the grain boundary mobility μ_{int} and grain boundary velocity v_{int} as

$$\mu_{\text{int}} = \frac{L}{g(\gamma)}\sqrt{\frac{\kappa}{m}}, \tag{11}$$

and

$$v_{\text{int}} = \mu_{\text{int}}\gamma_{\text{int}}\left(\frac{1}{\rho_1} + \frac{1}{\rho_2}\right) = L\kappa\left(\frac{1}{\rho_1} + \frac{1}{\rho_2}\right), \tag{12}$$

with $g(\gamma)$ a function of the model parameter γ [4]. For grain boundaries between grains of a different phase, the velocity depends on both the kinetics of the interfacial reactions (characterized by μ_{int}) and the diffusional transport of solutes. For the processes described in this paper, it can however be assumed that the movement of interfaces between different phases is diffusion controlled. L (or μ_{int}) is then taken large enough to obtain diffusion controlled interface movement, although not too large for numerical efficiency.

If cross interactions are ignored, the evolution of the composition fields $x_k(\mathbf{r},t)$ is given by diffusion equations of the form [5-8]

$$\frac{1}{V_m}\frac{\partial x_k}{\partial t} = \nabla \circ \sum_{\alpha} M_k(\vec{\eta})\nabla\frac{\partial f_b}{\partial x_k} = \nabla \circ \sum_{\rho} \phi_\rho M_k^\rho \nabla\vec{\mu}_k, \quad k = 1...C-1, \tag{13}$$

with

$$M_k^\rho = \frac{D_k^\rho}{\dfrac{\partial^2 G_m^\rho}{\partial x_k^2}}. \tag{14}$$

equations (14) reduce to the phenomenological diffusion equation of Fick.

With Gibbs energy expressions (15), constant parameter values for M_k^ρ result in constant diffusion coefficients D_k^ρ for the different bulk phases. For systems farther from thermodynamic equilibrium, it may be necessary to use directly the Gibbs energy expressions from the thermodynamic databases (instead of a parabolic approximation). Then, however, a more computationally intensive iterative procedure [7] is required to solve equations (8) and (9).

Parameter determination

For all interfaces, the parameters γ, κ, m and L are calculated iteratively for given interface energies γ_{int}, mobilities μ_{int} and a constant diffuse interface thickness ℓ_{gb}. The iterative procedure is described in [4] and implemented in Matlab.

If parabolic functions of the form

$$\frac{G_m^\rho}{V_m} = \sum_{k=1}^{C-1}\frac{A_k^\rho}{2}(x_k - x_{k,0}^\rho)^2 + C^\rho \tag{15}$$

with A_k^ρ, C_k^ρ and $x_{k,0}^\rho$ model parameters, are used for the Gibbs energies of the different phases, equations (8) and (9) result in a linear system of equations with the virtual composition fields as unknowns, which can be solved efficiently. The parameters in the parabolic Gibbs energy expressions (15) are obtained by fitting expressions (17) to Gibbs energy expressions from thermodynamic databases (obtained according to the CALPHAD method [9]) within the composition range of interest, namely around the equilibrium compositions of the coexisting phases. For $x_k < 10^{-12}$ or $x_k > 1 - 10^{-12}$, the A_k^ρ are taken 10 times larger than in the parabolic description fitted for phase ρ, to prevent the molar fraction of a component from taking an unphysical value beyond 0 or 1.

3. Diffusion and coarsening in Cu/Sn-0.02at%Cu solder joints

During soldering, typically an intermetallic compound (IMC) is formed between the molten solder and the solid substrate. Due to diffusion the IMC and intermetallic precipitates in the solder alloy continue to grow during device use. Because of their inherent brittle nature, the morphology and thickness/size of the IMC layer and precipitates strongly affect the mechanical properties of the solder joint.

Simulations were performed for a Cu-substrate / Sn-0.02at%Cu-solder joint annealed at about 180°C. A phase diagram of the Cu-Sn system is shown in Figure 2. The (Cu)-phase (fcc), the (Sn)-phase (bct) and the intermetallic Cu_6Sn_5-phase are considered in the simulations; the Cu_3Sn-phase is not considered for simplicity. The initial composition of the solder is close to the eutectic composition at which the solder solidifies. For all phases, the interfacial energy is taken $\gamma_{int} = 0.35$ J/m^2, the interface mobility $\mu = 3 \circ 10^2$ m^{2}s/kg and the diffuse interface width $\ell_{gb} = 5 \circ 10^{-7}$ m. Based on the phase diagram and existing Gibbs energy expressions (SSOL4 database [10]) for T*=180°C, the following parameters were chosen in the parabolic free ener-

gy expressions (15): $A^{(Cu)}=10^8$, $C^{(Cu)}=0$, $x_{0,Sn}^{(Cu)} = 0.076$, $A^{(Sn)} = 10^9$, $C^{(Sn)} = 10^7$, $x_{0,Sn}^{(Sn)}=0.979$, $A^{Cu6Sn5} = 10^{10}$, $C^{Cu6Sn5} = -10^6$, $x_{0,Sn}^{Cu6Sn5} = 0.455$. The parabolic free energies are plotted in Figure 3.

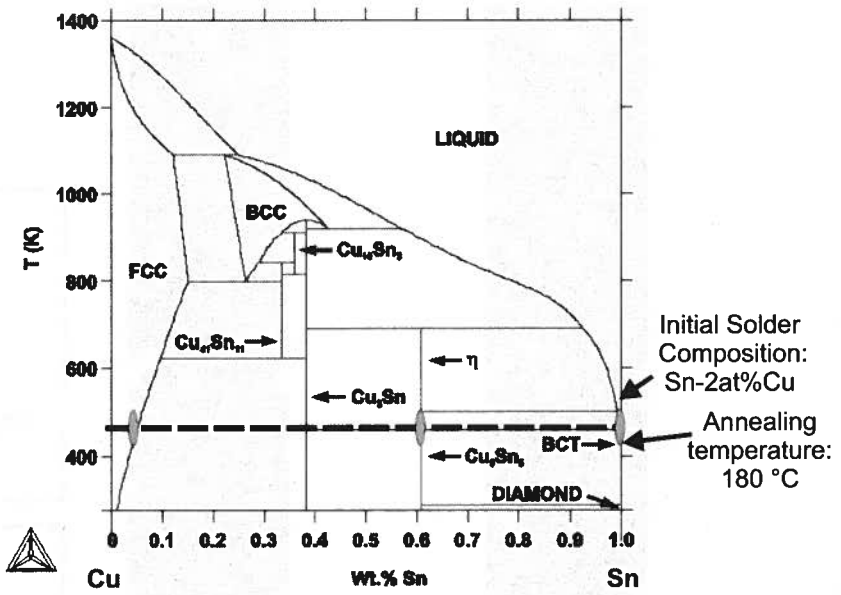

Fig. 2. Phase diagram of the Cu-Sn system. Relevant simulation conditions are indicated. The phases fcc-(Cu), Cu_6Sn_5 and bct-(Sn) are considered in the simulations

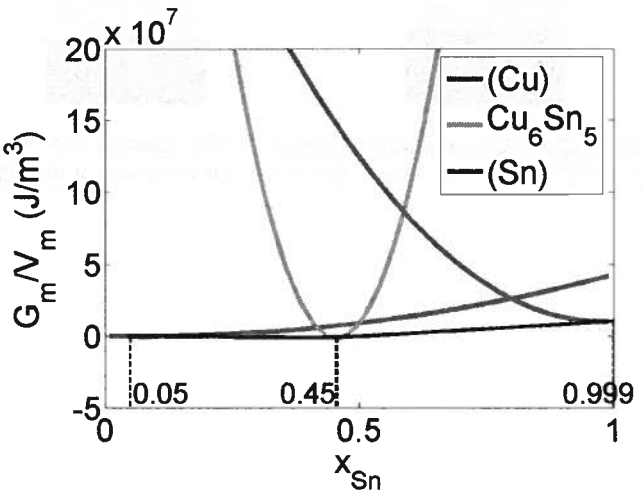

Fig. 3. Parabolic free energies for the (Cu), (Sn) and Cu_6Sn_5 phase used in the simulations of the lead-free solder joint. The equilibrium compositions of the coexisting phases, determined by the common tangent construction, are also indicated. The equilibrium compositions of the Cu_6Sn_5 phase with the (Cu) and (Sn) phase are near 0.45

Several simulation experiments were performed considering various values for the diffusion coefficients in the 3 phases. The initial compositions of the Cu_6Sn_5-phase and the (Sn)-phase were always taken close to their equilibrium composition, namely x_B = 0.9994 and x_B = 0.455 respectively. The initial (area) fraction of precipitates in a solder with composition $x_B = 0,98$ is accordingly 0.04. The initial composition of the (Cu)-phase varied between x_B = 0.001 (almost pure Cu substrate) and x_B = 0.05 (near equilibrium composition of (Cu)) for different simulation experiments.

The simulation images in Figure 4 show how the intermetallic Cu_6Sn_5-layer grows, consuming the (Cu) and (Sn) phases, by diffusion through the intermetallic layer. At the same time the intermetallic Cu_6Sn_5-precipitates undergo Ostwald ripening by Cu diffusion through the Sn-matrix. The volume fraction of the precipitates decreases in time as part of the Cu-atoms dissolved in the Sn-matrix re-precipitate on the intermetallic layer (and not on a precipitate). Finally, all precipitates vanish and deposite on the intermetallic layer.

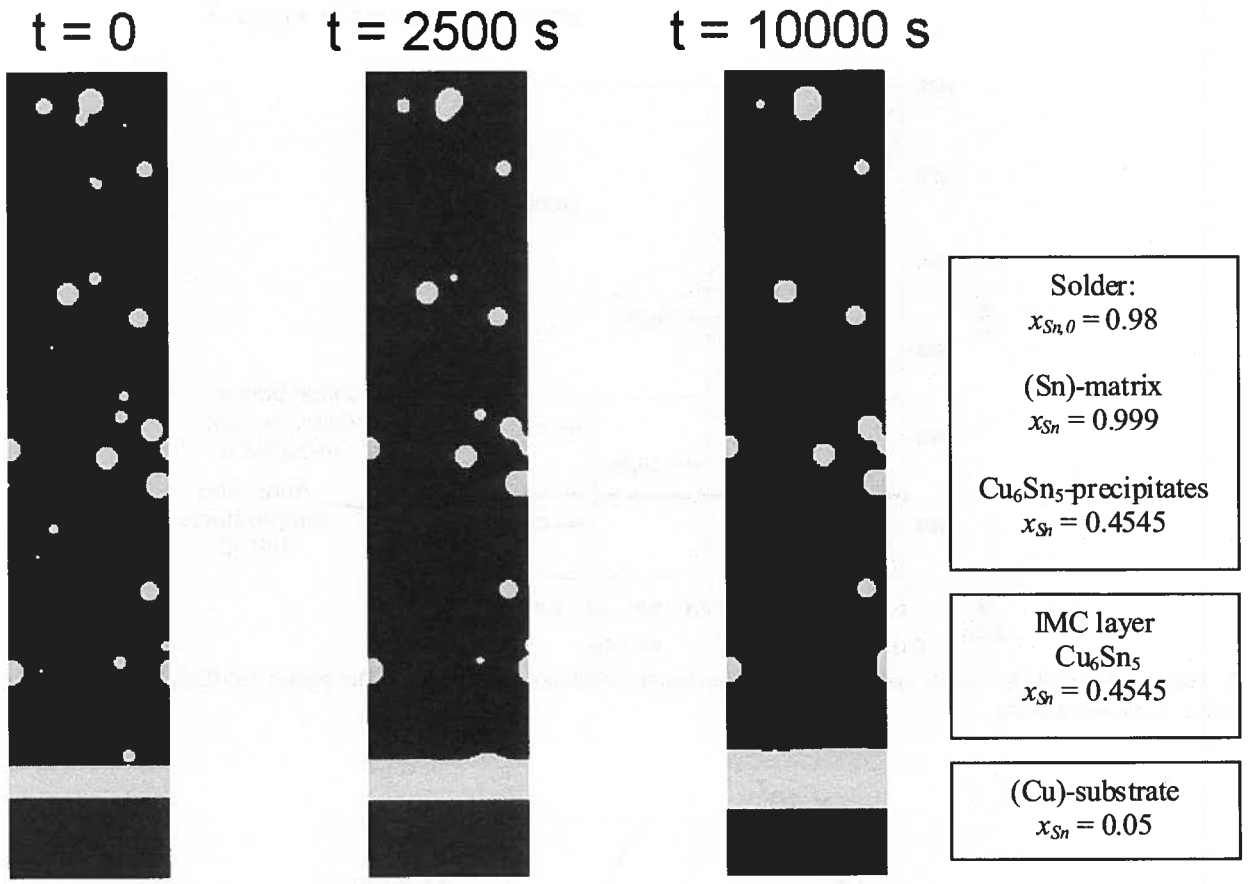

Fig. 4. Simulation images of the coarsening of a solder joint formed between a (Cu) substrate and Sn-0.02at%Cu solder for equal diffusion coefficients in all phases, $D_{Sn}^{Cu6Sn5} = D_{Sn}^{(Cu)} = D_{Sn}^{(Sn)} = 0.5 \circ 10^{-16}$ m²/s. The initial concentrations of the different phases are as indicated in the schematic picture on the right

In Figure 5, it is shown how the concentration profiles across the solder joint change in time for different diffusion parameters. In Figure 5a (equal diffusion coefficient in all phases), the Cu phase is first enriched with Sn while the intermetallic layer grows and the intermetallic precipitates coarsen. As long as the (Cu) phase is not saturated in Sn, the intermetallic layer grows into the solder, while it is consumed on the (Cu) side. Afterwards, the intermetallic layer grows symmetrically to both sides. For Figures 5b and 5c, diffusion in the (Cu) phase is several orders slower than in the (Sn) and Cu_6Sn_5 phase. As a consequence, the composition of the (Cu) phase remains almost constant. For Figure 5b, the diffusion coefficients of the (Sn) and Cu_6Sn_5 phase are of the same order of magnitude. The intermetallic layer then grows in both directions, although slightly faster into the solder. For Figure 5c, the diffusion coefficient of the Cu_6Sn_5 phase is several orders of magnitude smaller than that of the (Sn) phase. Then, the intermetallic layer grows mainly into the solder, as diffusion of Sn through the intermetallic layer is blocked due to the low diffusion coefficient. In all simulations, the smallest precipitates shrink and disappear and the larger precipitates grow.

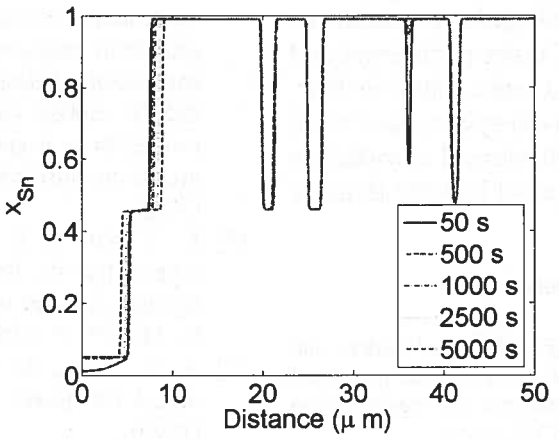

a)

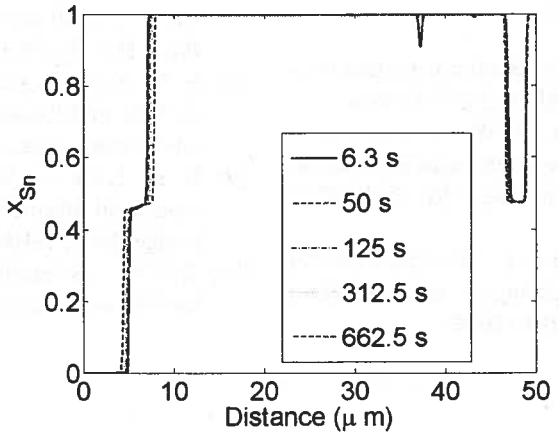

)

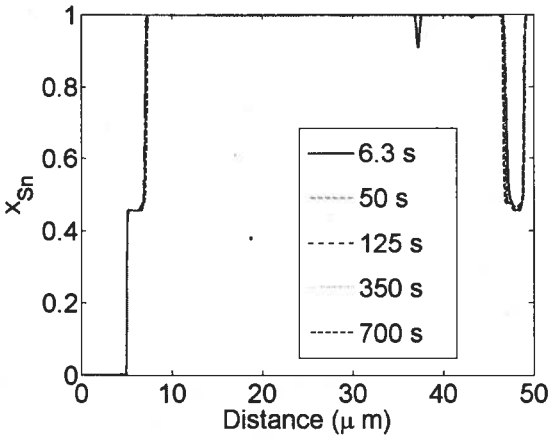

c)

Fig. 5. Concentration profiles across the solder joints at different times and obtained from different simulation experiments with initial composition of the Cu substrate equal to x_{Sn} = 0.001: (a) $D_{Sn}^{Cu6Sn5} = D_{Sn}^{(Cu)} = D_{Sn}^{(Sn)} = 0.5 \circ 10^{-13}$ m^2/s; (b) $D_{Sn}^{Cu6Sn5} = 0.5 \circ 10^{-13}$ m^2/s, $D_{Sn}^{(Cu)} = 0.5 \circ 10^{-25}$ m^2/s and $D_{Sn}^{(Sn)} = 0.5 \circ 10^{-12}$ m^2/s; (c) $D_{Sn}^{Cu6Sn5} = 0.5 \circ 10^{-16}$ m^2/s, $D_{Sn}^{(Cu)} = 0.5 \circ 10^{-25}$ m^2/s and $D_{Sn}^{(Sn)} = 0.5 \circ 10^{-12}$ m^2/s

4. Conclusions

In this paper, a novel phase field formulation for multi-component and multi-phase materials is introduced and applied to simulate the growth and coarsening of the intermetallic layer and precipitates in a simplified Cu-Sn solder joint. The effect of different values of the diffusion coefficients on the evolution of the composition profiles is examined.

It is straightforward to incorporate the Cu_3Sn phase

and extra components, for example Ag, in the model description in future work, but computer requirements will increase with the number of order parameters and composition fields. Furthermore, a more extensive literature study on diffusion in Cu-Sn(-X) systems and more experimental measurements and theoretical calculations of the diffusion properties are required in order to make simulations more predictive.

Acknowledgements

The author gratefully acknowledges FWO – Flanders and OT/07/040 for financial support. Part of the work was performed in the framework of COST MP0602. Simulations were performed on the High Performance Computer of the K.U.Leuven.

REFERENCES

[1] L.-Q. Chen, Phase-field models for microstructure evolution, Annu. Rev. Mater. Res. **32**, 113-140 (2002).

[2] K. Thornton, J. Agren, P. W. Voorhees, Modelling the evolution of phase boundaries in solids at the meso- and nano-scales, Acta Mater. **51**, 5675-5710 (2003).

[3] N. Moelans, B. Blanpain, P. Wollants, An introduction to phase field modeling of microstructure evolution, CALPHAD **32**, 268-294 (2008).

[4] N. Moelans, B. Blanpain, P. Wollants, Quantitative phase-field approach for simulating grain growth in anisotropic systems with arbitrary inclination and misorientation dependence, Phys. Rev. Lett. **101**, 025502 (2008); Quantitative analysis of grain boundary properties in a generalized phase field model for grain growth in anisotropic systems, Phys. Rev. B, **78**, 024113 (2008).

[5] J. Tiaden, B. Nestler, H. J. Diepers, I. Steinbach, The multiphase-field model with an integrated concept for modelling solute diffusion, Physica D, **115**, 73-86 (1998).

[6] S. G. Kim, W. T. Kim, T. Suzuki, Phase-field model for binary alloys, Phys. Rev. E, **60**, 7186-7196 (1999).

[7] J. Eiken, B. Böttger, I. Steinbach, Multiphase-field approach for multicomponent alloys with extrapolation scheme for numerical application, Phys. Rev. E, **73**, 066122 (2006).

[8] S. G. Kim, A phase-field model with antitrapping current for multicomponent alloys with arbitrary thermodynamic properties, Acta Mater. **55**, 4391-4399 (2007).

[9] H. L. Lukas, S. G. Fries, B. Sundman, Computational thermodynamics: The Calphad Method, Cambridge 2007, ISBN 0-08-0421296.

[10] SGTE (Scientific Group Thermodata Europe), http://www.sgte.org/

Received: 10 August 2008.